Solvation, Solute Rotation and Vibration Relaxation, and Electron-Transfer Reactions in Room-Temperature Ionic Liquids

YOUNGSEON SHIM,[†] DAUN JEONG,[‡] SWATI MANJARI,[†] MOO YOUNG CHOI,[‡,§] AND HYUNG J. KIM*[,†,||]

Department of Chemistry, Carnegie Mellon University, Pittsburgh, Pennsylvania 15213, Department of Physics and Astronomy, Seoul National University, Seoul 151-747, Korea, School of Physics, Korea Institute for Advanced Study, Seoul 130-722, Korea, and Department of Physics, Korea University, Seoul 136-701, Korea

Received March 13, 2007

ABSTRACT

A brief account of recent simulation and theoretical model studies of various solution-phase processes in room-temperature ionic liquids is given. These include structure and dynamics of equilibrium and nonequilibrium solvation, solute rotation and vibrational energy relaxation, and free energetics and dynamics of unimolecular electron-transfer reactions. Special attention is paid to both the aspects shared by and the contrasts with polar solvents under normal conditions. A brief comparison with available experiments is also made.

1. Introduction

Recently, ionic liquids based on bulky and asymmetric cations, e.g., *N,N*′-dialkylimidazolium and *N*-alkylpyridinium, paired with a variety of different anions have been the subject of intensive study because of their exciting potential as a "green" alternative to toxic organic solvents and a wide range of materials and device applications.[1] This class of systems exists as a liquid at or near room temperature; hence, they are often referred to as room-temperature ionic liquids (RTILs). RTILs are usually nonvolatile, nonflammable, and thermally stable. Therefore, volatile products of chemical synthesis can be separated completely through distillation, and RTILs can be recycled. This helps to reduce toxic wastes significantly. Because of their high intrinsic conductivity and wide electrochemical window as well as nonvolatility, RTILs also provide an excellent candidate for an electrolyte in electrochemical devices, such as batteries and solar cells.

The last few years have seen significant progress in unraveling important details of physicochemical properties of RTILs, thanks to extensive experimental and theoretical studies. For differing aspects of these efforts, the reader is referred to many excellent Accounts in this issue of *Accounts of Chemical Research.* Our own efforts have been focussed mainly on gaining a fundamental understanding of solvation and related processes in RTILs at the microscopic level via molecular dynamics (MD) computer simulations and theoretical modeling. These include structure and dynamics of equilibrium and nonequilibrium solvation,[2–5] rotational[6] and vibrational energy[7] relaxation, and chemical reactions involving charge shift and transfer.[8] In this Account, we present a brief overview of these studies and elucidate similarities and differences between polar solvents and RTILs. We give only certain highlights of our results. For details, the reader is referred to the original works.[2–8]

The outline of this Account is as follows: In section 2, a brief explanation of models and methods employed in our study of 1-ethyl-3-methylimidazolium hexafluorophosphate ($EMI^+PF_6^-$) is given. Solvation structure and dynamics in $EMI^+PF_6^-$ are analyzed in section 3. Effective polarity is also considered there. We examine solute rotational dynamics and related dynamic heterogeneity in $EMI^+PF_6^-$ in section 4 and vibrational energy relaxation in section 5. Free energetics and dynamics of unimolecular electron transfer are considered in section 6. Section 7 concludes this Account.

2. Models and Methods

We begin with a brief description of models employed in our MD simulations. We use a simple diatomic solute as a probe for solvation and related processes in $EMI^+PF_6^-$.

Youngseon Shim was born in Incheon, Korea, in 1977. She received her Ph.D. degree in physics from Seoul National University in 2005. She is currently a postdoctoral research associate in the Department of Chemistry at Carnegie Mellon University. Her research interest is the computational study of solvation and chemical reactions in ionic liquids and polar solvents.

Daun Jeong was born in Jeongeup, Korea, in 1979. She completed her doctorate degree in physics at Seoul National University in 2007. She currently holds a postdoctral position in the Chemistry Department at Seoul National University. Her research focus is the dynamics of ionic liquids and self-assembled peptide amphiphiles.

Swati R. Manjari was born in Delhi, India, in 1976. She completed her Ph.D. degree in chemistry at Carnegie Mellon University in 2006. She is currently studying solvation dynamics in bulk and confined room-temperature ionic liquids using molecular simulations as a postdoctoral researcher in the Department of Chemistry at Carnegie Mellon University.

Moo Young Choi was born in Seoul, Korea, in 1957. After he received his Ph.D. degree in physics from Stanford University in 1984, he worked at Ohio State University as a postdoctoral researcher. Since 1987, he has been on the faculty of Seoul National University, where he is currently a Professor of Physics. He also holds a position of Affiliated Professor at Korea Institute for Advanced Study. His research interest spans phase transitions and dynamics of complex systems, physics of biological systems, and mesoscopic quantum phenomena.

* To whom correspondence should be addressed. E-mail: hjkim@cmu.edu.

[†] Carnegie Mellon University.

[‡] Seoul National University.

[§] Korea Institute for Advanced Study.

[||] Korea University.

Hyung J. Kim was born in Seoul, Korea, in 1956. After he completed his graduate research in chemical physics at the State University of New York (SUNY) at Stony Brook in 1988, he did postdoctoral research in the Department of Chemistry and Biochemistry at the University of Colorado, Boulder, CO. In 1992, he joined the faculty of Carnegie Mellon University, where he is currently a Professor of Chemistry. He is also an adjunct faculty member of the Department of Physics, Korea University. His research theme centers around equilibrium and nonequilibrium statistical mechanics of solution systems and chemical reaction dynamics in condensed phases.

10.1021/ar700061r CCC: $37.00
Published on Web 08/18/2007

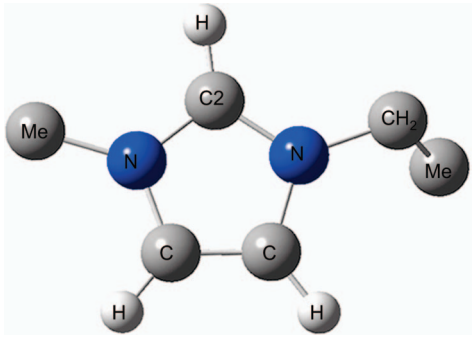

FIGURE 1. EMI^+ ion.

Two constituent solute atoms, separated by 3.5 Å, are identical except for their charge assignments q. Three different charge distributions are considered: a neutral pair (NP) with no charges, an ion pair (IP) with $q = \pm e$, and their intermediate state (HIP) with $q = \pm 0.5e$, where e is the elementary charge.

We describe solute electronic structure variations needed in the analysis of solvation and electron transfer using two nonpolarizable electronic states a and b that are degenerate in energy (a,b = NP,IP). For a given solvent configuration Q and a solute electronic state i (=a,b), the total energy of the solute–solvent system is denoted as $E_i(Q)$. The Franck–Condon (FC) energy $\Delta E_{a\rightarrow b}(Q)$ associated with the $a \rightarrow b$ transition

$$\Delta E_{a\rightarrow b}(Q) = E_b(Q) - E_a(Q) \qquad (1)$$

measures the difference in the solvent-induced stabilization of states a and b, which varies with Q. Thus, $\Delta E_{a\rightarrow b}$ is widely employed to describe the collective influence of the solvent on the solute. The average FC energy

$$\langle \Delta E_{a\rightarrow b} \rangle = \int \mathrm{d}Q f_a^{\mathrm{eq}}(Q) \Delta E_{a\rightarrow b}(Q) \qquad (2)$$

determined with equilibrium ensemble distribution $f_a^{\mathrm{eq}}(Q)$ in the presence of the a-state solute describes the solvation-stabilization difference between a and b associated with the steady-state $a \rightarrow b$ transition.

All simulations in $EMI^+PF_6^-$ were conducted in the canonical ensemble at temperature $T = 400$ K using the DL_POLY program.[9] A united-atom representation was employed for CH_2 and CH_3 moieties of EMI^+ (Figure 1) as well as for PF_6^-. For a comparison, we also simulated acetonitrile and water systems at room temperature using the model descriptions of refs 10 and 11, respectively. For details of the simulations and potential models, the reader is referred to refs .2–8

3. Solvation Structure and Dynamics

Solute–solvent electrostatic interactions play a central role in solvation in polar solvents. These interactions induce the reorientation of solvent dipoles ("polarization") and enhance local solvent density ("electrostriction") around a polar solute, compared to a nonpolar solute (see Figure 2 below). This reorganization of solvent molecules is fundamental to, e.g., charge-transfer reactions and related spectroscopies in solution. RTILs are another solvent class where the solute–solvent electrostatic interactions can be

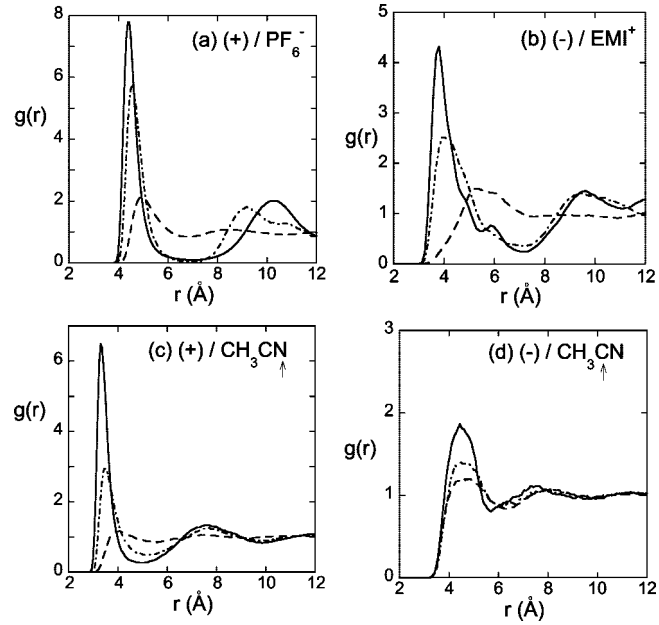

FIGURE 2. Solvent radial distribution functions around the solute. Distributions of anions and centers of cations in $EMI^+PF_6^-$ around, respectively, the (a) positively and (b) negatively charged sites of IP (—), HIP (-•-), and a neutral site of NP (- - -) are shown. $g(r)$ of N and central C of acetonitrile around the solute (+) and (−) sites are presented in c and d, respectively. In b, the cation center is defined as the midpoint of two N atoms of the imidazole ring of EMI^+ (Figure 1).

of primary importance. To obtain a molecular-level understanding of the roles played by these interactions in RTILs, we first investigate the structure and dynamics of solvation in $EMI^+PF_6^-$ and their variations with solute electronic structure.

Structure and Effective Polarity. Radial distribution functions $g(r)$ of anions and cations around, respectively, the positively and negatively charged sites of diatomic solutes in $EMI^+PF_6^-$ are exhibited in Figure 2. For a comparison, $g(r)$ of the nitrogen atom with a partial negative charge and $g(r)$ of the central carbon atom with a partial positive charge of solvent molecules in acetonitrile are also shown. There is pronounced structure-making in both solvents as the solute charge separation increases. Solvent anions (cations) in $EMI^+PF_6^-$ are brought in closer to the positive (negative) site of the solute, and their local density grows as the solute dipole moment increases ("electrostriction").[2,3,8,12] Similar trends are obtained in acetonitrile. Although not presented here, anisotropy in the angular distributions of solvent ions around the solute increases markedly as its charge distribution changes from NP to IP in RTILs.[3] We thus expect that charge shift and transfer processes in RTILs will be accompanied by significant reorganization of solvent ions, analogous to polar solvents. It is worthwhile to note that the overall extent of solvation structure variations is more pronounced in $EMI^+PF_6^-$ than in acetonitrile. For instance, $g(r)$ for the central carbon of acetonitrile (Figure 2d), located close to the molecular center of mass, does not vary much with the solute charge distribution despite its partial positive charge, while $g(r)$ for centers of anions

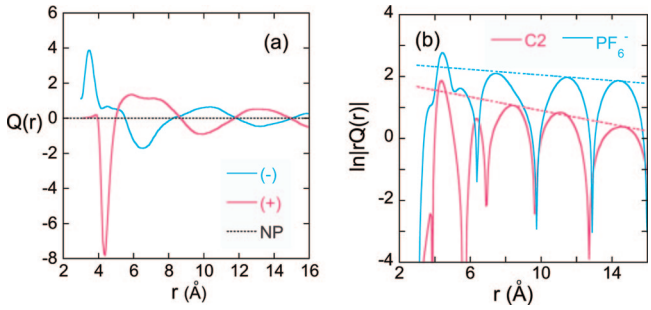

FIGURE 3. Local charge density $Q(r)$ around various sites of the (a) solute and (b) solvent in $EMI^+PF_6^-$.

Table 1. Simulation Results[a]

solvent	T (K)	density	$\langle \Delta E_{NP\rightarrow IP} \rangle$
EMI^+Cl^-	400	1.1	100.6
$EMI^+PF_6^-$	400	1.31	83.8
$EMI^+PF_6^-$	400	1.375	94.1
CH_3CN	300	0.73	76.5
water	298	0.998	121.2

[a] Units: g/cm^3 (density) and kcal/mol (energy).

(Figure 2a) and cations (Figure 2b) in $EMI^+PF_6^-$ show marked structural enhancement as the solute dipole grows.[8] A likely reason is that EMI^+ and PF_6^- can be displaced independent of each other as long as the overall electroneutrality condition is met, whereas the positively and negatively charged sites of an acetonitrile molecule cannot.

Figure 3a shows the local charge densities $Q(r)$ around the solute in $EMI^+PF_6^-$. While $Q(r) = 0$ nearly everywhere around NP, the cation-rich/anion-deficient and anion-rich/cation-deficient regions alternate around IP. Thus, in addition to electrostriction, solute–solvent electrostatic interactions result in the (smeared-out) separation of cations and anions in RTILs, while they lead to the reorientation of solvent dipoles in polar solvents. The overall amplitudes of $Q(r)$ diminish as the distance r from IP increases. The peak positions of $Q(r)$ generally agree with those of corresponding $g(r)$ in Figure 2. To gain further insight, we analyze our results via

$$Q(r) = \frac{A}{r} e^{-r/\lambda} \sin\left(\frac{2\pi r}{d} + \phi\right) \tag{3}$$

originally developed for strongly coupled simple ionic systems.[13] Here, λ is the screening length, and d and φ are the period and phase associated with charge oscillations, respectively. We estimate $\lambda \sim 10$ and $d \sim 6$ Å for $Q(r)$ around IP. For charge densities around solvent ions (Figure 3b), eq 3 yields $\lambda \approx 10$ Å for various sites of EMI^+ and ~20 Å for PF_6^-. Similar results were obtained for other RTILs.[3,14] Because of the large size of solvent ions, the screening length in RTILs is rather long.

We turn to effective polarity, which gauges the power of solvents of solvating polar solutes. Experimentally, the effective polarity is often measured as solvent-induced shifts of absorption spectra of polar chromophores, e.g., $E_T(30)$ and Kosower Z factors.[15] Empirical polarity scales thus obtained are very similar to $\langle \Delta E_{IP\rightarrow NP} \rangle$ in eq 2. The results in Table 1 indicate that, insofar as their solvating capabilities are concerned, RTILs behave as a more polar

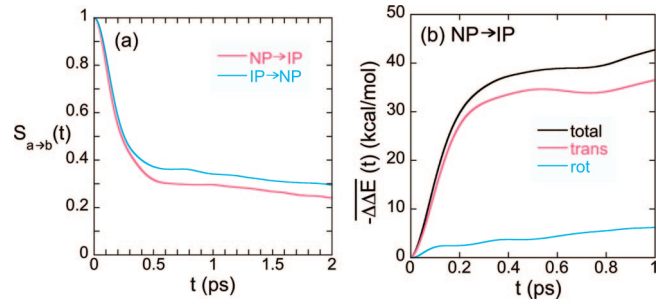

FIGURE 4. (a) Dynamic Stokes shift $S_{a\rightarrow b}(t)$ and (b) contributions from solvent rotational and translational motions to $\overline{\Delta E_{NP\rightarrow IP}}(t)$ in $EMI^+PF_6^-$ ($\Delta\Delta E_{a\rightarrow b}(t) \equiv \overline{\Delta E_{a\rightarrow b}}(t) - \overline{\Delta E_{a\rightarrow b}}(0)$). $\overline{\Delta E_{IP\rightarrow NP}}(t)$ (not presented here) shows a very similar behavior.

solvent than acetonitrile, consonant with solvatochromic measurements.[16] Although their dielectric constants are not high ($\varepsilon \approx 10$),[17,18] the monopolar charge character of constituent ions of RTILs allows strong electrostatic interactions with and thus leads to substantial solvation stabilization of solute charge distributions. Nonetheless, they are not as polar as water.

Dynamics. The normalized dynamic Stokes shift

$$S_{a\rightarrow b}(t) = \frac{\overline{\Delta E_{a\rightarrow b}}(t) - \overline{\Delta E_{a\rightarrow b}}(\infty)}{\overline{\Delta E_{a\rightarrow b}}(0) - \overline{\Delta E_{a\rightarrow b}}(\infty)} \tag{4}$$

is widely used to describe solvation dynamics. In eq 4, $\overline{\Delta E_{a\rightarrow b}}(t)$ is the average FC energy associated with $a \rightarrow b$ at time t after an instantaneous change in the solute electronic structure from the charge distribution of b to that of a and the average is over the initial distribution of solvent configurations in equilibrium with the b-state solute. MD results in Figure 4a show that $S_{a\rightarrow b}(t)$ is characterized by at least two vastly different dynamics, ultrafast subpicosecond relaxation and extremely slow nonexponential decay.[4,5] The former is attributed mainly to small-amplitude inertial translations of ions (see below), and the latter is attributed to ion transport via diffusion.[2,4] Perhaps, the most notable aspect of Figure 4a is the prominent role of the ultrafast dynamics. Despite its relatively high viscosity, more than 60% of the entire $S_{a\rightarrow b}(t)$ relaxation in $EMI^+PF_6^-$ occurs via ultrafast dynamics in the first ~0.5 ps! Other related RTILs show similar behavior.[4,19] This state of affairs is generally in good agreement with time-resolved spectroscopy measurements.[20–26]

To understand molecular motions responsible for $S_{a\rightarrow b}(t)$, we consider respective contributions of solvent translations and rotations to $\overline{\Delta E_{a\rightarrow b}}(t)$. Figure 4b shows that translation dynamics account for almost 90% of the overall solvent relaxation.[4] Thus, ion translations play a dominant role in solvation dynamics in RTILs in contrast to molecular rotations in polar solvents under normal conditions.

We proceed to solvent structural relaxation[4] in Figure 5, where time evolution of anion radial distributions around the solute (+) site subsequent to solute FC transitions is shown. In Figure 5a, the solvent, initially equilibrated to the IP solute, relaxes to a new state in equilibrium with NP. In the first ~0.2 ps, there are hardly any changes in the

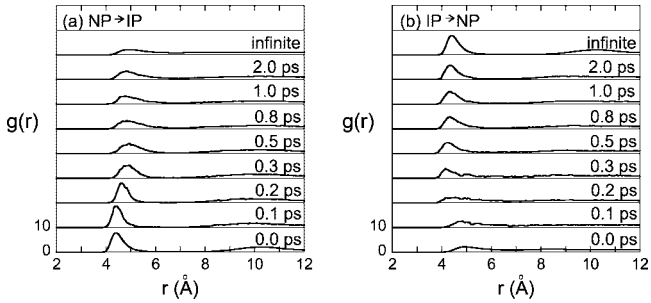

FIGURE 5. Relaxation of radial distributions of PF_6^- subsequent to instantaneous changes in the solute charge distribution in $EMI^+PF_6^-$. Distributions in a and b represent structural relaxation accompanying $S_{NP\rightarrow IP}(t)$ and $S_{IP\rightarrow NP}(t)$, respectively.

solvation structure. The only noticeable change is in the first solvation shell, the peak of which shifts from $r \approx 4.4$ to 4.6 Å. According to Figure 4a, however, this very minor structural change accounts for ~50% of $S_{NP\rightarrow IP}(t)$ relaxation. The corresponding change in energy is ~30 kcal/mol (Figure 4b). To understand this, we consider the anion coordination number n_A, defined as the number of PF_6^- located within 6 Å from the solute (+) site. At $t = 0$, the anion coordination number is $n_A = 4.3$. If we assume that the average separation between the solute (+) site and PF_6^- in its first solvation shell increases from 4.4 to 4.6 Å during the first 0.2 ps, then the magnitude of their electrostatic interaction energy decreases by ~14 kcal/mol. Thus, the anions in the first solvation shell alone can account for nearly 50% of the energy relaxation during ~0.2 ps. This indicates that short-time relaxation of $S_{NP\rightarrow IP}(t)$ arises predominantly from motions of a few ions close to the solute and thus does not provide an accurate measure for solvation structure changes.[4]

The overall trend in Figure 5b is similar to that in Figure 5a. Structural changes in the first ~0.2 ps are nearly insignificant, while corresponding relxation in $S_{IP\rightarrow NP}(t)$ is very substantial. This again shows that the ultrafast component of dynamic Stokes shifts is not a proper indicator of accompanying solvation structure changes. Despite their similarities, however, there is one important difference between the two cases of Figure 5. Because initial ion coordination numbers are low, e.g., $n_A = 2.8$, in Figure 5b (cf. $n_A = 4.3$ in Figure 5a), the ions close to the solute alone are not sufficient to account for the ultrafast energy relaxation of a large magnitude associated with $S_{IP\rightarrow NP}(t)$. Thus, ions in regions located farther from the solute than its first solvation shell play a more significant role in the subpicosecond relaxation of $S_{IP\rightarrow NP}(t)$ than the $S_{NP\rightarrow IP}(t)$ case.[4]

We turn to equilibrium solvation dynamics.[2,3,5,19,27–29] MD results for the normalized time correlation function (TCF)

$$C_{a\rightarrow b}(t) \equiv \frac{\langle \delta\Delta E_{a\rightarrow b}(0)\delta\Delta E_{a\rightarrow b}(t)\rangle}{\langle (\delta\Delta E_{a\rightarrow b})^2\rangle} \qquad \delta\Delta E_{a\rightarrow b}(t) = \Delta E_{a\rightarrow b}(t) - \langle \Delta E_{a\rightarrow b}\rangle \quad (5)$$

in Figure 6a show that characteristics of $C_{a\rightarrow b}(t)$ are very close to those of $S_{a\rightarrow b}(t)$, including two distinct dynamic regimes, the importance of ultrafast relaxation and the

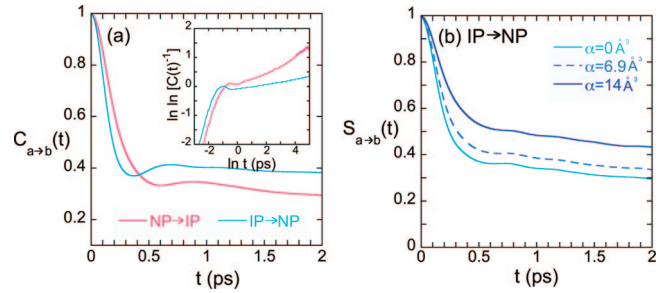

FIGURE 6. (a) $C_{a\rightarrow b}(t)$ in $EMI^+PF_6^-$. (b) Solute polarizability effect on $S_{IP\rightarrow NP}(t)$ (α = solute polarizability along its molecular axis).

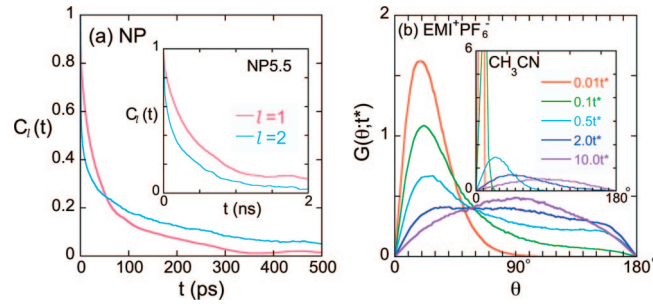

FIGURE 7. (a) $C_l(t)$ for NP and NP5.5 in $EMI^+PF_6^-$. (b) $G(\theta;t^*)$ ($t^* \equiv t/\tau_R^{(2)}$) for NP in $EMI^+PF_6^-$ and in acetonitrile.

nonexponential behavior of long-time decay. Also noteworthy is that the long-time relaxation of $C_{a\rightarrow b}(t)$ is reasonably described as a stretched exponential function.[2,4] Its implications will be considered in section 4 below.

Finally, we consider the effect of solute polarizability on solvation dynamics.[5] According to MD results in Figure 6b, qualitative aspects of $S_{a\rightarrow b}(t)$ remain unaffected with the inclusion of the a-state polarizability. Quantitatively, increasing the a-state polarizability tends to reduce the contribution of ultrafast solvation dynamics to $S_{a\rightarrow b}(t)$. Similar results are obtained for $C_{a\rightarrow b}(t)$. This generally yields a better agreement with experiments.[26] This trend of solvation dynamics with solute polarizability was first found in the MD study of water.[30]

4. Rotational Dynamics

In this section, we examine solute rotational dynamics in $EMI^+PF_6^-$ via TCFs $C_l(t)$ and correlation time $\tau_R^{(l)}$

$$C_l(t) = \langle P_l[\cos\theta(t)]\rangle \qquad \tau_R^{(l)} = \int_0^\infty dt C_l(t) \quad (6)$$

where P_l is the lth order Legendre polynomial and $\theta(t)$ is the angle between the solute molecular axis at time t and its initial direction.

Figure 7a displays MD results on $C_l(t)$ for NP.[6] Its reorientational TCFs show a bimodal character, viz., relatively fast relaxation for $t \lesssim 1$ ps, followed by slow decay. The long-time relaxation shows a stretched exponential behavior $\exp[-(t/\tau_l)^{\beta_l}]$ for 2 ps $\lesssim t \lesssim$ 1 ns ($\beta_1 = 0.54$, $\tau_1 = 32$ ps, and $\beta_2 = 0.27$, $\tau_2 = 12$ ps). This is in line with polarization anisotropy decay measurements.[23,31] The stretched exponential behavior, also observed in $C_{a\rightarrow b}(t)$ above, is suggestive of dynamic heterogeneity (see below).[32] Perhaps most striking is that the long-time decay of $C_2(t)$ is slower than that of $C_1(t)$, whereas the opposite

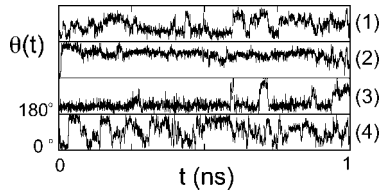

FIGURE 8. $\theta(t)$ for NP in $EMI^+PF_6^-$ for different 1 ns segments of the MD trajectory.[6]

trend results at short times. As a consequence, $C_1(t)$ and $C_2(t)$ intersect at $t \approx 60$ ps. Their correlation times are $\tau_R^{(1)} \approx 50$ and $\tau_R^{(2)} \approx 100$ ps, i.e., $\tau_R^{(1)} < \tau_R^{(2)}$. This reveals that NP rotations in $EMI^+PF_6^-$ do not fall in the regular diffusion regime (see below).

To investigate the solute size effect on rotational dynamics, we studied another nonpolar diatomic solute (NP5.5) with a bond length of 5.5 Å. Its mass is adjusted, so that its moment of inertia is the same as that of NP with a bond length of 3.5 Å. $C_l(t)$ of the bigger NP5.5 in the inset of Figure 7 shows more diffusion-like character than those of the smaller NP. For example, $C_l(t)$ of NP5.5 relaxes faster as l increases; thus, no crossing is observed. Reorientations of NP5.5, although nonexponential, are closer to a single exponential than those of NP. This is another indirect evidence for dynamic heterogeneity in RTILs. Because of different length scales associated with locally heterogeneous environments, the range of heterogeneity accessible via a probe solute and its influence on rotational dynamics diminish as the solute size grows.[32] A similar dependence of $C_l(t)$ on the probe size was observed experimentally in RTILs.[23]

For a better understanding of $C_l(t)$, we consider conditional probability

$$G(\theta;\, t) = \langle\, \delta(\theta(t) - \theta)\,\rangle = \sum_l \frac{2l+1}{2} P_l(\cos\theta)\sin\theta C_l(t) \tag{7}$$

associated with solute reorientation. We notice in Figure 7b that the main peak of $G(\theta;\, t)$ near $\theta = 20°$ hardly moves, while its amplitude decreases with t. Thus, on average, solute molecules are trapped in this orientation for a long time. Another pronounced feature is that $G(\theta;\, t)$ develops a shoulder structure around $\theta = 160°$. (A similar structure was observed in reorientations of solvent ions in RTILs.)[33,34] In contrast, solute rotations in acetonitrile (inset) do not show this structure. Because the shoulder structure becomes stronger with t, the probability of finding NP at large θ becomes enhanced in $EMI^+PF_6^-$ compared with the normal solvents, especially at long times. The enhanced probability for $\theta > 90°$ tends to decrease $C_l(t)$ for odd l and thus accelerate its relaxation at later times because $\cos\theta < 0$. $C_l(t)$ with even l on the other hand is insensitive to the sign of $\cos\theta$, so that the probability enhancement at large θ does not accelerate their long-time relaxation. This differing influence of probability enhancement at large θ is responsible for the crossing of $C_1(t)$ and $C_2(t)$ in Figure 7a.

For further insight, four different 1 ns segments of the 60 ns equilibrium trajectory for NP rotations are presented in Figure 8. Subtrajectories 1 and 2 represent, respectively, fast and slow dynamics close to rotational diffusion.

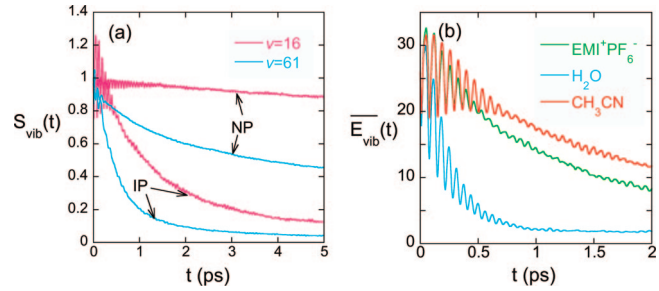

FIGURE 9. (a) $S_{vib}(t)$ of NP and IP in $EMI^+PF_6^-$. (b) Comparison of VER of IP in $EMI^+PF_6^-$ at 400 K and in acetonitrile and water at 298 K ($v = 16$).

Subtrajectory 3 depicts extremely slow rotation; the solute is nearly frozen at $\theta \approx 40°$ for more that 600 ps. In contrast, the solute in 4 undergoes frequent rotations of large amplitude. The marked diversity in characteristics of these long subtrajectories indicates that NP rotations in RTILs are hardly homogeneous. It suggests heterogeneous dynamics,[32] some evidence of which was also observed in other simulations[14,33–35] and experiments.[25,36,37] Nevertheless, in view of the crossing of $C_1(t)$ and $C_2(t)$, the prevalent notion that single-exponential relaxation results in a given local environment and superposition of many different exponentials leads to a stretched exponential behavior does not apply to solute rotational dynamics in RTILs.[6]

5. Vibrational Energy Relaxation

As another illustration of importance of solvent influence on solute dynamics, we consider vibrational energy relaxation (VER). We employ flexible diatomic solutes with a Morse potential

$$V(r) = D[e^{-\gamma(r-r_0)} - 1]^2 \qquad \mu\omega_0^2 = 2D\gamma^2$$
$$E_v = \hbar\omega_0\left(v + \frac{1}{2}\right)\left[1 - \frac{\hbar\omega_0}{4D}\left(v + \frac{1}{2}\right)\right] \tag{8}$$

to compute the normalized VER function $S_{vib}(t)$ and average relaxation time $\overline{T}_1$

$$S_{vib}(t) = \frac{\overline{E_{vib}}(t) - \overline{E_{vib}}(\infty)}{\overline{E_{vib}}(0) - \overline{E_{vib}}(\infty)} \qquad \overline{T}_1 = \int_0^\infty dt S_{vib}(t) \tag{9}$$

where $\overline{E_{vib}}(t)$ is the average vibrational energy at time t after the initial exciation of the solute from its ground to excited vibrational state with quantum number v. In eq 8, μ and r are the solute-reduced mass and bond length, ω_0 is the frequency at the minimum of $V(r)$ and E_v is the vibrational energy eigenvalue. In the simulations, the zero-point energy was neglected and $\mu = 7.5$ amu, $D = 100$ kcal/mol, and $\gamma = 1.0735$ Å^{-1} were employed, so that $\omega_0 = 600$ cm^{-1}.

Results for $S_{vib}(t)$ in $EMI^+PF_6^-$ are presented in Figure 9a. One of the salient features is that VER of IP is much faster than that of NP. For the $v = 16$ initial state, $\overline{T}_1$ is ~51 ps for NP, while it is much shorter (3.2 ps) for IP. For $v = 61$, $\overline{T}_1 \approx 14$ and 1.0 ps, respectively. Similar trends were found previously in normal polar solvents.[38] The acceleration of VER with an increasing solute charge

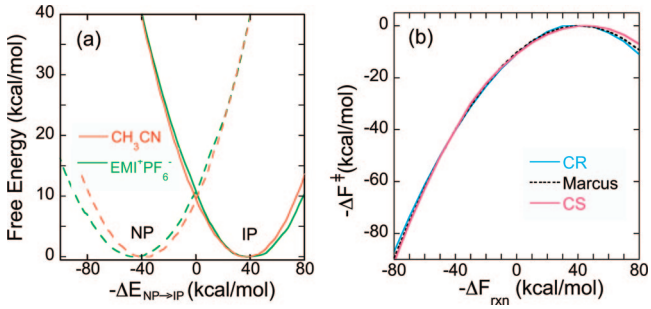

FIGURE 10. (a) Diabatic free-energy curves for CS/CR in $EMI^+PF_6^-$ at 400 K and CH_3CN at 298 K. The IP curve is shifted, so that the reaction is thermoneutral. (b) $\Delta F^{\ddagger}$ versus ΔF_{rxn} in $EMI^+PF_6^-$.

separation is usually attributed to electrostriction.[7,39,40] The solvent density enhancement near the solute with an increasing solute dipole (cf. Figure 2) strengthens the short-range solute–solvent interactions and, as a consequence, enhances spatial variations of the force and thus friction on the solute vibrations exerted by the solvent. Another noteworthy feature is that $\overline{T}_1$ varies with the initial excitation energy; VER from the $v = 61$ state is faster than that from $v = 16$, by a factor of ~3 for both the IP and NP solutes. This mainly arises from the increase in vibrational amplitudes with growing v, which in turn enhances the variations of the solvent force on the solute bond and thus accelerates VER.[7]

In Figure 9b, VER in $EMI^+PF_6^-$ is compared with that in water and acetonitrile.[7] Basic qualitative aspects of VER are similar among three solvents, including the acceleration of VER (results not shown here) with an increasing solute dipole and growing initial v. Quantitatively, $\overline{T}_1$ in $EMI^+PF_6^-$ is close to that in acetonitrile, while water shows much faster VER. This is in good accordance with recent measurements with small anionic solutes.[41]

6. Electron-Transfer Reaction

We now turn to electron-transfer (ET) reactions[42–46] in $EMI^+PF_6^-$, in particular, unimolecular charge separation and recombination (CS/CR) processes NP ⇌ IP.

ET Free Energetics. The diabatic free-energy curves for the NP and IP states in $EMI^+PF_6^-$ and acetonitrile determined with the free-energy perturbation method[47] along $\Delta E_{NP\to IP}$ are compared in Figure 10a.[8] Overall characteristics of the NP and IP curves are similar between the two solvents. While both curves are anharmonic, their anharmonicity is not that strong for $-40 \lesssim \Delta E_{NP\to IP} \lesssim 40$ kcal/mol. We also observe that the NP curve is wider than IP, especially in $EMI^+PF_6^-$. In ref 3, this curvature difference was ascribed to electrostriction-induced enhancement in the rigidity of the solvent structure near the solute as the solute dipole increases. As a result, the solvent reorganization free energy λ varies with the solute electronic state. In $EMI^+PF_6^-$, the reorganization free energies defined on the NP and IP curves are, respectively, $\lambda_{NP} = 38$ kcal/mol and $\lambda_{IP} = 44$ kcal/mol. The corresponding values in acetonitrile are $\lambda_{NP} = 36$ kcal/mol and $\lambda_{IP} = 38$ kcal/mol. The λ_{IP}–λ_{NP} difference in $EMI^+PF_6^-$ is considerably larger than that in acetonitrile. This is probably closely related to huge electrostrictive effects in the former observed in Figure 2 above.

Figure 10b displays variations of the ET barrier height $\Delta F^{\ddagger}$ with the free energy of the reaction ΔF_{rxn} in $EMI^+PF_6^-$. For a comparison, the Marcus theory[48] predictions

$$\Delta F^{\ddagger} = \frac{(\Delta F_{rxn} + \lambda_{av})^2}{4\lambda_{av}} \tag{10}$$

are also presented, where $\lambda_{av} = (\lambda_{NP} + \lambda_{IP})/2$ is employed as the solvent reorganization free energy. Overall, the Marcus theory describes free energetics of CS/CR in $EMI^+PF_6^-$ reasonably well. Considering dramatic electrostrictive effects in RTILs, this level of agreement is quite remarkable. Nevertheless, the discrepancy between the MD and Marcus theory becomes substantial when ET becomes strongly exo- or endothermic. For instance, the onset of the inverted regime for CS is $\Delta F_{rxn} = -44$ kcal/mol, whereas it starts at $\Delta F_{rxn} = -38$ kcal/mol for CR. Thus, the difference in free energetics between CS and CR in the inverted regime is not negligible, and the Marcus theory with λ_{av} fails to capture this. For acetonitrile, we note that eq 10 holds very well, except for highly endo- or exothermic cases because its λ_{IP}–λ_{NP} difference is small.

ET Dynamics. We proceed to ET barrier-crossing dynamics. If the magnitude of electronic coupling between the diabatic states is larger than k_BT (k_B = Boltzmann's constant), ET is well-described as activated barrier crossing on a single electronic curve. If solvent relaxation in the reactant and product wells is fast, the barrier crossing is rate-limiting. In this case, the ET rate k_{ET} becomes

$$k_{ET} \approx k_b = \kappa k_{TST} \qquad k_{TST} = \frac{\omega_{s,R}}{2\pi}\exp[-\Delta F^{\ddagger}/k_BT] \tag{11}$$

where k_b is the barrier crossing rate and $\omega_{s,R}$ is the solvent frequency in the reactant well. The transmission coefficient κ measures the deviation of k_b induced by solvent dynamics in the barrier region from the transition-state theory (TST) prediction k_{TST}.

In the Grote–Hynes (GH) theory,[49] where the reactive mode is described via the generalized Langevin equation, the transmission coefficient is given by the self-consistent equation

$$\kappa_{GH} = \left[\kappa_{GH} + \frac{\tilde{\zeta}(\omega_b\kappa_{GH})}{\omega_b}\right]^{-1} \tag{12}$$

where ω_b is the barrier frequency, $\zeta(t)$ is the time-dependent solvent friction in the barrier region, and $\tilde{\zeta}(\omega)$ is its Laplace transform

$$\tilde{\zeta}(\omega) = \int_0^\infty dt\zeta(t)e^{-\omega t} \qquad \tilde{\zeta}(0) = \int_0^\infty dt\zeta(t) \tag{13}$$

Thus, barrier-crossing dynamics in the GH theory are governed by the friction at the reactive frequency $\kappa_{GH}\omega_b$. In the limit of slow barrier crossing, eq 12 reduces to the Kramers (KR) theory,[50] i.e., $\kappa_{KR} = -(\tilde{\zeta}(0)/2\omega_b) + [(\tilde{\zeta}(0)/2\omega_b)^2 + 1]^{1/2}$, where barrier crossing is determined by the total friction $\tilde{\zeta}(0)$.

Because the determination of $\zeta(t)$ in the unstable barrier region is not amenable, we instead use the friction defined in a stable solvent well.[51] Results for $\zeta(t)$ thus

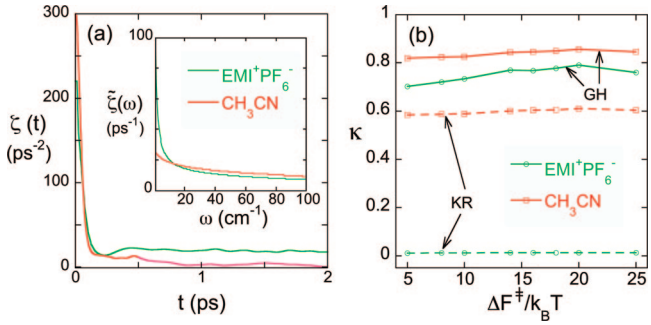

FIGURE 11. (a) Time-dependent friction and (b) transmission coefficient for ET in $EMI^+PF_6^-$ and CH_3CN. In b, 2 kcal/mol was employed for electronic coupling between the IP and NP states.

obtained are exhibited in Figure 11a.[4] Similar to solvation dynamics in section 3 above, $\zeta(t)$ shows bimodal relaxation. The long-time decay of $\zeta(t)$ in $EMI^+PF_6^-$ is extremely slow, while its relaxation in acetonitrile is completed in 1–2 ps. Because of a huge memory effect in $EMI^+PF_6^-$, its total friction is about 50 times higher than that of acetonitrile. Their respective $\tilde{\xi}(0)$ values are 1300 and 27 ps^{-1}. Despite this startling difference in overall friction, $\tilde{\xi}(\omega)$ values of the two solvents become similar for $\omega \gtrsim 10$ cm^{-1}. This means that for solvent-collective motions faster than ~10 cm^{-1}, the properties of dissipative dynamics will be more or less the same between the two solvents!

Results for κ_{GH} and κ_{KR} are compared in Figure 11b.[8] We notice that the GH and KR predictions for the ET rate are comparable in acetonitrile. A similar agreement between the two was observed previously in CH_3Cl.[51] In contrast, the GH and KR results in $EMI^+PF_6^-$ are totally different; κ_{GH} is larger than κ_{KR} by nearly 2 orders of magnitude! The main reason for this discrepancy is that the friction relevant to barrier crossing, i.e., $\tilde{\xi}(\omega)$ at the reactive frequency $\kappa_{GH}\omega_b$, is smaller than the total friction by 2 decades. To be specific, $\tilde{\xi}(\kappa_{GH}\omega_b) \approx 9$ ps^{-1} ($\kappa_{GH}\omega_b \approx 50$–$100$ cm^{-1}), while $\tilde{\xi}(0) = 1300$ ps^{-1}. Because of erroneous inclusion of the large contribution from the long-time friction, the KR description based on $\tilde{\xi}(0)$ drastically underestimates κ and k_{ET} in $EMI^+PF_6^-$. Thus, it would be totally incorrect to assume that the Kramers theory would apply to RTILs simply because it works well for polar solvents of similar effective polarity.

Another important feature is that TST provides a reasonable framework for ET kinetics not only in acetonitrile but also in $EMI^+PF_6^-$. The k_{ET} results with account of barrier-crossing dynamics agree with the TST predictions within a factor of ~2. Although we do not discuss it here, the inclusion of activation/deactivation dynamics does not affect this state of affairs significantly.[8] This could have an important bearing on other systems, e.g., isomerization reactions,[52,53] whose kinetics in RTILs were found to be considerably faster than estimated on the basis of viscosity.

7. Concluding Remarks

In this Account, we have presented a brief review of our recent efforts to gain a theoretical understanding of solvation and related processes in RTILs. Despite a number of apparent similarities to normal polar solvents, we have found that RTILs are quite unique in many respects in both structure and dynamics. Specifically, the imidazolium-based RTILs studied here show high effective polarity and large electrostriction. Their solvation dynamics span a wide range of differing time scales. Despite their high viscosity, short-time solvation dynamics are in the subpicosecond regime and make a major contribution to the overall relaxation. Their long-time dynamics, on the other hand, are close to a stretched exponential decay. A similar nonexponential behavior is also found in rotational dynamics of small nonpolar solutes. This indicates that RTILs are dynamically heterogeneous. Another interesting finding is that the TST provides a good framework to describe activated ET in RTILs, even though they are much more viscous than normal polar solvents. Thus, continued efforts of both theory and experiments will be definitely worthwhile and desirable to unveil molecular details of a wide range of differing solution-phase processes in RTILs and to elucidate their sometimes intriguing and anomalous behaviors.

Many works presented here were supported in part by KOSEF through the National Core Research Center for Systems Bio-Dynamics and by NSF Grant CHE-0098062.

References

(1) For recent reviews, see, e.g., Welton, T. Ionic Liquids in Catalysis. *Coord. Chem. Rev.* **2004**, *248*, 2459–2477. Zhang, Z. C. Catalysis in Ionic Liquids. *Adv. Catal.* **2006**, *49*, 153–237. Dupont, J.; Suarez, P. A. Z. Physico-chemical Processes in Imidazolium Ionic Liquids. *Phys. Chem. Chem. Phys.* **2006**, *8*, 2441–2452.
(2) Shim, Y.; Duan, J.; Choi, M. Y.; Kim, H. J. Solvation in Molecular Ionic Liquids. *J. Chem. Phys.* **2003**, *119*, 6411–6414.
(3) Shim, Y.; Choi, M. Y.; Kim, H. J. A Molecular Dynamics Computer Simulation Study of Room-Temperature Ionic Liquids: I. Equilibrium Solvation Structure and Free Energetics. *J. Chem. Phys.* **2005**, *122*, 044510/12.
(4) Shim, Y.; Choi, M. Y.; Kim, H. J. A Molecular Dynamics Computer Simulation Study of Room-Temperature Ionic Liquids: II. Equilibrium and Nonequilibrium Solvation Dynamics. *J. Chem. Phys.* **2005**, *122*, 044511/12.
(5) Jeong, D.; Shim, Y.; Choi, M. Y.; Kim, H. J. Effects of Solute Electronic Polarizability on Solvation in a Room-Temperature Ionic Liquid. *J. Phys. Chem. B* **2007**, *111*, 4920–4925.
(6) Shim, Y.; Jeong, D.; Choi, M. Y.; Kim, H. J. Rotational Dynamics of a Diatomic Solute in the Room-Temperature Ionic Liquid 1-Ethyl-3-methylimidazolium Hexafluorophosphate. *J. Chem. Phys.* **2006**, *125*, 061102/4.
(7) Shim, Y.; Kim, H. J. Vibrational Energy Relaxation of a Diatomic Molecule in a Room-Temperature Ionic Liquid. *J. Chem. Phys.* **2006**, *125*, 024507/14.
(8) Shim, Y.; Kim, H. J. Free Energy and Dynamics of Electron Transfer Reactions in a Room-Temperature Ionic Liquid. *J. Phys. Chem. B* **2007**, *111*, 4510–4519.
(9) Forster, T. R.; Smith, W. *The DL_POLY_2.13 Reference Manual*; CCLRC Daresbury Laboratory: Warington, U.K., 2001.
(10) Edwards, D. M. F.; Madden, P. A.; McDonald, I. R. A Computer Simulation Study of the Dielectric Properties of a Model of Methyl Cyanide: I. The Rigid Dipole Case. *Mol. Phys.* **1984**, *51*, 1141–1161.
(11) Berendsen, H. J. C.; Postma, J. P. M.; von Gunsteren, W. F.; Hermans, J. Interaction Models for Water in Relation to Protein Hydration. In *Intermolecular Forces*; Pullman, B., Eds.; Reidel: Dordrecht, The Netherlands, 1981; pp 331–342.

(12) Hanke, C. G.; Johansson, A.; Harper, J. B.; Lynden-Bell, R. M. Why Are Aromatic Compounds More Soluble Than Aliphatic Compounds in Dimethylimidazolium Ionic Liquids? A Simulation Study. *Chem. Phys. Lett.* **2003**, *374*, 85–90.
(13) See, e.g., Stell, G. New Results on Some Ionic-Fluid Problems. In *New Approaches to Problems in Liquid State Theory: Inhomogeneities and Phase Separation in Simple, Complex and Quantum Fluids*; Caccamo, C., Hansen, J. P., Stell, G., Eds.; Kluwer: Dordrecht, The Netherlands, 1999; pp 71–89.
(14) Del Pópolo, M. G.; Voth, G. A. On the Structure and Dynamics of Ionic Liquids. *J. Phys. Chem. B* **2004**, *108*, 1744–1752.
(15) See, e.g., Reichardt, C. *Solvents and Solvent Effects in Organic Chemistry*, 2nd ed.; Verlag Chemie: Weinheim, Germany, 1988.
(16) For an extensive list of references on solvatochromic measurements in RTILs, see ref 8.
(17) Daguenet, C.; Dyson, P. J.; Krossing, I.; Oleinikova, A.; Slattery, J.; Wakai, C.; Weingärtner, H. Dielectric Response of Imidazolium-Based Room-Temperature Ionic Liquids. *J. Phys. Chem. B* **2006**, *110*, 12682–12688.
(18) Wakai, C.; Oleinikova, A.; Ott, M.; Weingärtner, H. How Polar Are Ionic Liquids? Determination of the Static Dielectric Constant of an Imidazolium-Based Ionic Liquid by Microwave Dielectric Spectroscopy. *J. Phys. Chem. B* **2005**, *109*, 17028–17030.
(19) Margulis, C. J. Computational Study of Imidazolium-Based Ionic Solvents with Alkyl Substituents of Different Lengths. *Mol. Phys.* **2004**, *102*, 829–838.
(20) Karmakar, R.; Samanta, A. Solvation Dynamics of Coumarin-153 in a Room-Temperature Ionic Liquid. *J. Phys. Chem. A* **2002**, *106*, 4447–4452.
(21) Chakrabarty, D.; Hazra, P.; Chakarborty, A.; Seth, D.; Sarkar, N. Dynamics of Solvent Relaxation in Room Temperature Ionic Liquids. *Chem. Phys. Lett.* **2003**, *381*, 697–704.
(22) Chowdhury, P. K.; Halder, M.; Sanders, L.; Calhoun, T.; Anderson, J. L.; Armstrong, D. W.; Song, X.; Petrich, J. W. Dynamic Solvation in Room-Temperature Ionic Liquids. *J. Phys. Chem. B* **2004**, *108*, 10245–10255.
(23) Ito, N.; Arzhantsev, S.; Maroncelli, M. The Probe Dependence of Solvation Dynamics and Rotation in the Ionic Liquid 1-Butyl-3-methyl-imidazolium Hexafluorophosphate. *Chem. Phys. Lett.* **2004**, *396*, 83–91.
(24) Lang, B.; Angulo, G.; Vauthey, E. Ultrafast Solvation Dynamics of Coumarin 153 in Imidazolium-Based Ionic Liquids. *J. Phys. Chem. A* **2006**, *110*, 7028–7034.
(25) Samanta, A. Dynamic Stokes Shift and Excitation Wavelength Dependent Fluorescence of Dipolar Molecules in Room Temperature Ionic Liquids. *J. Phys. Chem. B* **2006**, *110*, 13704–13716.
(26) Arzhantsev, S.; Jin, H.; Ito, N.; Maroncelli, M. Observing the Complete Solvation Response of DCS in Imidazolium Ionic Liquids, from the Femtosecond to Nanosecond Regimes. *Chem. Phys. Lett.* **2006**, *417*, 524–529.
(27) Kobrak, M. N.; Znamenskiy, V. Solvation Dynamics of Room-Temperature Ionic Liquids: Evidence for Collective Solvent Motion on Sub-picosecond Timescales. *Chem. Phys. Lett.* **2004**, *395*, 127–132.
(28) Bhargava, B. L.; Balasubramanian, S. Dynamics in a Room-Temperature Ionic Liquid: A Computer Simulation Study of 1,3-Dimethylimidazolium Chloride. *J. Chem. Phys.* **2005**, *123*, 144505/8.
(29) Kobrak, M. N. Characterization of the Solvation Dynamics of an Ionic Liquid via Molecular Dynamics Simulation. *J. Chem. Phys.* **2006**, *125*, 064502/11.
(30) Bursulaya, B. D.; Zichi, D. A.; Kim, H. J. Role of Solute Electronic Polarizability in Solvation Dynamics. *J. Phys. Chem.* **1995**, *99*, 10069–10074.
(31) Arzhantsev, S.; Ito, N.; Heitz, M.; Maroncelli, M. Solvation Dynamics and Rotation of Coumarin 153 in Alkylphosphonium Ionic Liquids. *J. Phys. Chem. B* **2004**, *108*, 5771–5777.
(32) See Richert, R. Heterogeneous Dynamics in Liquids: Fluctuations in Space and Time. *J. Phys.: Condens. Matter* **2002**, *14*, R703–R738, and references therein.
(33) Ribeiro, M. C. C. Translational and Reorientiational Heterogeneity in the Glass-Forming Liquid $Ca_{0.4}K_{0.6}(NO_3)_{1.4}$. *Phys. Chem. Chem. Phys.* **2004**, *6*, 771–774.
(34) Hu, Z.; Margulis, C. J. Heterogeneity in a Room-Temperature Ionic Liquid: Persistent Local Environments and the Red-Edge Effect. *Proc. Natl. Acad. Sci. U.S.A.* **2006**, *103*, 831–836.
(35) Cadena, C.; Zhao, Q.; Snurr, R. Q.; Maginn, E. J. Molecular Modeling and Experimental Studies of the Thermodynamic and Transport Properties of Pyridinium-Based Ionic Liquids. *J. Phys. Chem. B* **2006**, *110*, 2821–2832.
(36) Cang, H.; Li, J.; Fayer, M. D. Orientational Dynamics of the Ionic Organic Liquid 1-Ethyl-3-methylimidazolium Nitrate. *J. Chem. Phys.* **2003**, *119*, 13017–13023.
(37) Mandal, P. K.; Sarkar, M.; Samanta, A. Excitation Wavelength Dependent Fluorescence Behavior of Some Dipolar Molecules in Room Temperature Ionic Liquids. *J. Phys. Chem. A* **2004**, *108*, 9048–9053.
(38) For an extensive list of references on VER in polar solvents, see ref 7.
(39) Bruehl, M.; Hynes, J. T. Vibrational Relaxation Times for a Model Hydrogen-Bonded Complex in a Polar Solvent. *Chem. Phys.* **1993**, *175*, 205–221.
(40) Ladanyi, B. M.; Stratt, R. M. On the Role of Dielectric Friction in Vibrational Energy Relaxation. *J. Chem. Phys.* **1999**, *111*, 2008–2118.
(41) Dahl, K.; Sando, G. M.; Fox, D. M.; Sutto, T. E.; Owrutsky, J. C. Vibrational Spectroscopy and Dynamics of Small Ions in Ionic Liquid Solutions. *J. Chem. Phys.* **2005**, *123*, 084504/11.
(42) Gordon, C. M.; McLean, A. J. Photoelectron Transfer from Excited-State Ruthenium(II) Tris(bipyridyl) to Methylviologen in an Ionic Liquid. *Chem. Commun.* **2000**, 1395–1396.
(43) Behar, D.; Gonzalez, C.; Neta, P. Reaction Kinetics in Ionic Liquids: Pulse Radiolysis Studies of 1-Butyl-3-methylimidazolium Salts. *J. Phys. Chem. A* **2001**, *105*, 7607–7614.
(44) McLean, A. J.; Muldoon, M. J.; Gordon, C. M.; Dunkin, I. R. Bimolecular Rate Constants for Diffusion in Ionic Liquids. *Chem. Commun.* **2002**, 1880–1881.
(45) Alvaro, M.; Ferrer, B; Garcia, H.; Narayana, M. Screening of an Ionic Liquid as Medium for Photochemical Reactions. *Chem. Phys. Lett.* **2002**, *362*, 435–440.
(46) Skrzypczak, A.; Neta, P. Diffusion-Controlled Electron-Transfer Reactions in Ionic Liquids. *J. Phys. Chem. A* **2003**, *107*, 7800–7803.
(47) King, G.; Warshel, A. Investigation of the Free Energy Functions for Electron Transfer Reactions. *J. Chem. Phys.* **1990**, *93*, 8682–8692.
(48) Marcus, R. A. Electrostatic Free Energy and Other Properties of States Having Nonequilibrium Polarization. I. *J. Chem. Phys.* **1956**, *24*, 966–978. Marcus, R. A. Electrostatic Free Energy and Other Properties of States Having Nonequilibrium Polarization. I*. *J. Chem. Phys.* **1956**, *24*, 979–989.
(49) Grote, R. F.; Hynes, J. T. The Stable States Picture of Chemical Reactions. II. Rate Constants for Condensed and Gas Phase Reaction Models. *J. Chem. Phys.* **1980**, *73*, 2715–2732.
(50) Kramers, H. A. Brownian Motion in a Field of Force and the Diffusion Model of Chemical Reactions. *Physica* **1940**, *7*, 284–304.
(51) Zichi, D. A.; Ciccotti, G.; Hynes, J. T.; Ferrario, M. Molecular Dynamics Simulation of Electron-Transfer Reactions in Solution. *J. Phys. Chem.* **1989**, *93*, 6261–6265.
(52) Ozawa, R.; Hamaguchi, H. Does Photoisomerization Proceed in an Ionic Liquid. *Chem. Lett.* **2001**, 736–737.
(53) Gutkowski, K. I.; Japas, M. L.; Aramenda, P. F. Fluorescence of Dicyanovinyl Julolidine in a Room-Temperature Ionic Liquid. *Chem. Phys. Lett.* **2006**, *426*, 329–333.

AR700061R